




Nanoscale light field imaging with graphene

Tongcheng Yu¹, Francisco Rodriguez¹, Fred Schedin², Vasyl G. Kravets¹, Vladimir A. Zenin ³, Sergey I. Bozhevolnyi ³, Konstantin S. Novoselov ^{1,4} & Alexander N. Grigorenko¹✉

Modern nano-optics and nanophotonics rely heavily on the precise formation of nanostructured light fields. Accurate and deterministic light field formation and characterization are indispensable for device operation as well as for revealing the underlying physical mechanisms involved. Despite a significant progress made in detection of scattered light with extremely high precision down to 1 nm resolution, there are only a limited number of techniques for direct subwavelength light mapping which do not rely on measurements of light scattering, fluorescence, or non-linear light conversion. Hence, techniques for direct conversion of light to electrical signals with precise and non-destructive imaging of nanoscale light would be of great benefit. Here, we report a nanoscale light field imaging approach based on photodetection with a *p-n* junction that is induced and moved inside a graphene probe by gate voltage, formed by a set of external electrodes. The spatial resolution of this electrical scanning technique is determined by *p-n* junction width, reaching ~ 20 nm. The developed approach is demonstrated with mapping the electric field distribution of a plasmonic slot-waveguide at telecom wavelengths. Our method provides a non-invasive nanoscale light field imaging that ensures extremely high spatial resolution and precision.

¹ Department of Physics and Astronomy, University of Manchester, Oxford Road, Manchester M13 9PL, UK. ² National Graphene Institute, University of Manchester, Oxford Road, Manchester M13 9PL, UK. ³ Centre for Nano Optics, University of Southern Denmark, Campusvej 55, DK-5230 Odense, Denmark. ⁴ Department of Materials Science and Engineering, National University of Singapore, Singapore 117574, Singapore. ✉email: alexander.grigorenko@manchester.ac.uk

Nanoscale light manipulation and characterization are two pillars of modern nano-optics^{1–3}. Recently, a significant progress in this field has been realized through the use of plasmonic structures⁴ and their assemblies^{5–7}, superlenses^{8,9}, plasmonic waveguides¹⁰, graphene plasmonics^{11,12}, and optical phononics¹³. At the same time, most often the light field imaging and characterization still rely on microscopy methods: detection of scattered propagating optical fields that are subject to the diffraction limit, thus limiting the spatial resolution to a fraction of the light wavelength¹⁴. The resolution of light field imaging can be significantly improved by utilizing optical near-fields¹⁵. Unfortunately, the near-field optical microscopy suffers from the fundamental six-power scaling of scattered power with the probe size¹⁶ that limits the resolution in practice for direct light mapping to the level of 50 nm at optical wavelengths^{17,18}. The archetypal near-field microscopy is also inherently invasive as the detected optical fields are scattered by a probe immersed in an interrogated optical (near) field. Moreover, the workhorse of modern near-field optical characterization, scattering scanning near-field optical microscopy (s-SNOM) with pseudo-heterodyne interferometric detection¹⁷, utilizes demodulation of detected signals at high harmonics to suppress the background, a very efficient approach that however introduces inevitably image distortions when fields with different spatial frequencies are being imaged.

It should be mentioned that there have been developed various electron microscopies, such as electron energy-loss spectroscopy (EELS) and cathodoluminescence (CL) microscopy, that provide information on the optical response of nanostructures with unmatched, down to sub-nanometre, spatial resolutions by making use of tightly focused electron beams¹⁸. The optical information is deduced by analyzing spatial maps of correspondingly electron energy loss spectra or spectra of emitted radiation, mapping the efficiency of resonant excitation of hybrid polariton modes, and relating the efficiency maps to the mode spatial distributions. The electron microscopies provide thereby indirect access to the optical information, and one has to use elaborate data treatment to extract this information and mainly that associated with resonant excitations¹⁸.

Indirect methods of light imaging using scattered fields can also achieve extremely high spatial resolution down to 1 nm. For example, mapping of Brownian motion of a dye particle was used to image fluorescent profile of a single hot spot with 1 nm resolution¹⁹, surface-enhanced Raman scattering can be used to evaluate electric fields with high spatial resolution of 5 nm, see review²⁰, backscattered light can be used to determine optical oscillation patterns of plasmon modes with the help of s-SNOM achieving resolution of <10 nm²¹. However, these indirect methods (while providing extremely high spatial resolution) are often invasive and rely on certain assumptions which allow one to translate measured parameters to light field maps.

Here we describe a conceptually different direct and virtually non-invasive method of nanoscale light-field imaging with a lateral resolution of ~20 nm. The method is based on the photoelectric effect in a *p-n* junction induced in graphene. The position of such *p-n* junction can be very accurately controlled by an external gate voltage. The graphene surface defines the plane of optical field imaging and should thus be placed near a nanostructure generating nanoscale light fields to be characterized. As a practical example, we measure the electric field profile of a strongly confined plasmonic slot-waveguide mode at telecom wavelengths. The experimentally obtained mode profile is found to be in excellent agreement with numerical simulations. Our method provides a practical way of nanoscale light field imaging with extremely high spatial resolution and precision. It should be emphasized that, in terms of the optical information made available, our approach is similar to conventional near-field

microscopy techniques^{15,17}, but, being radically different in the operation principle, allows one to circumvent the aforementioned fundamental limitation in the achievable spatial resolution. It is worth stressing that light field imaging discussed in this work is concerned with non-destructive mapping of optical fields with direct conversion of light to electrical signals. The limitations of our method in the presented form are connected to the complex fabrication procedures and limited geometries which can be probed. We believe that these limitations can be overcome with technique development.

Results

Nanoscale mapping of light fields with graphene. The concept of nanoscale mapping of light fields with the help of graphene is illustrated in Fig. 1 (here we consider one-dimensional light field imaging for simplicity). A graphene sheet is placed in the region of interest and electrically connected with source and drain contacts. It is important that the source and drain contacts are made from the same material and are kept at the same temperature to avoid thermopower parasitic signals. Gate dielectric is deposited on top of graphene, and two parallel metallic gates are fabricated on top of the dielectric, defining the orientation of a *p-n* junction and, thus, the scanning direction (parallel and perpendicular to the gate electrodes, respectively). Note that the two-dimensional light imaging with this concept is, in principle, feasible, but would require a more complex gating arrangement.

When the area between the two gating contacts is exposed to light—an additional electrical signal is observed in graphene. Here, it is worth mentioning that graphene absorption in the visible and near-infrared light is ~2.3% at normal incidence²² and at the level of 0.01–0.1 dB· μm^{-1} for confined plasmonic modes propagating along the graphene layer²³, so that the influence of graphene on light field distributions can be neglected. There are several phenomena that could contribute to the electrical signal: the photoelectric²⁴, thermoelectric²⁵, and bolometric²⁶ effects. While the bolometric effect should be zero in non-biased graphene²⁶, both the photoelectric and thermoelectric effects could, in general, contribute to the electrical signal induced by light illumination and provide the possibility for the electrical detection of light fields. It is often assumed that the thermoelectric effect yields the largest contribution²⁶. However, in the case when the source and the drain are kept at the same temperature and made of the same material, it is possible to show that the total thermoelectric contribution is exactly zero for metals²⁷ (see also Supplementary Note 1). The exception to this rule is a discontinuity in temperature derivative²⁸ or dependence of the mean free path of electrons on the wavevector²⁷. For semiconductors, the situation is more complicated and the contribution of the thermoelectric effect could be non-zero. In the following, we will assume that the main contribution to the photo-electrical signal in our case comes from the photoelectric effect, which requires the presence of a *p-n* junction in graphene to separate electrons and holes produced during light absorption.

The above consideration suggests the following method of nanoscale light field imaging. Initially, doped graphene (e.g., *p*-doped) is gated by the gating contact with a positively applied voltage V_{G2} while the other contact is connected to ground ($V_{G1} = 0$) in such a way that a *p-n* junction is formed in the area where the light is present (see Fig. 1a). A non-zero photoelectric current is thereby generated, with the current being proportional to the electric field intensity at the position of the *p-n* junction where the electron–hole pairs produced by light are separated due to the electric field applied. Variation of Fermi energy across a *p-n* junction induced in graphene in our geometry (Fig. 1b) was calculated for the 30 nm-thin hafnia dielectric separator using the

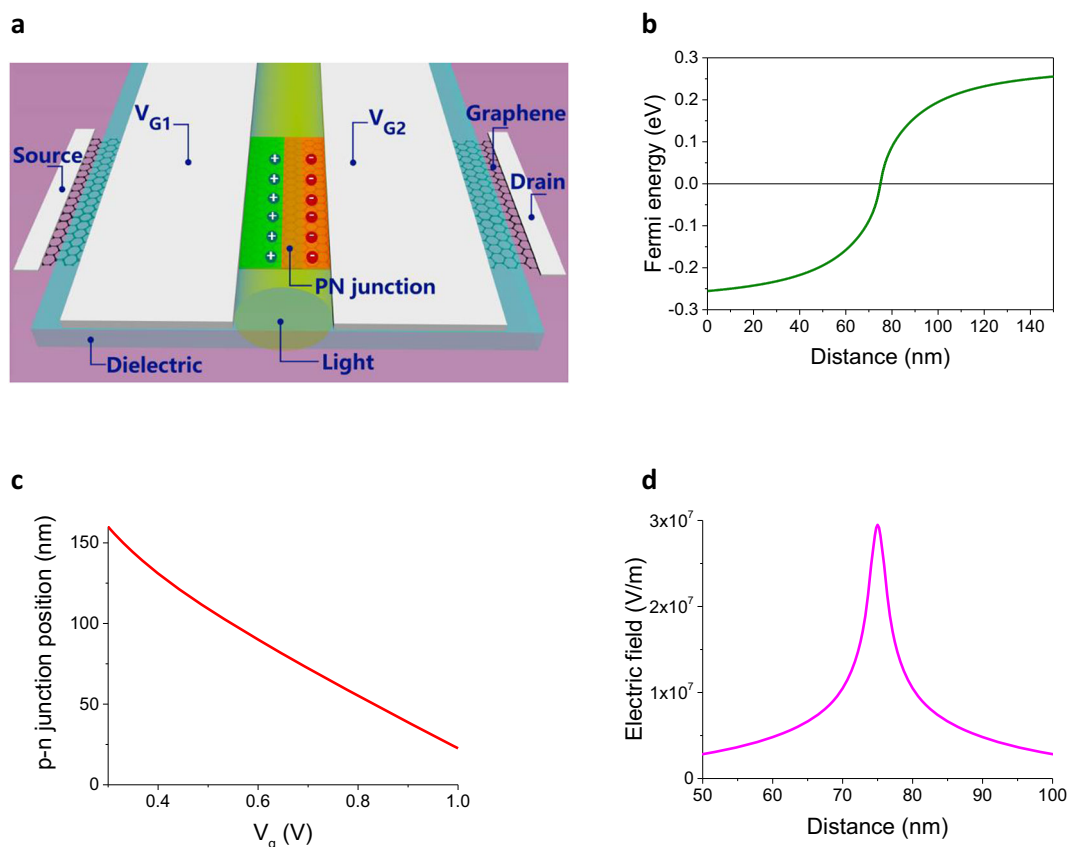


Fig. 1 Electric detection of light fields. **a** Schematics of a *p-n* junction induced in graphene by gating of a plasmonic waveguide. **b** Fermi energy in initially doped graphene calculated in the presence of a gate voltage applied to one side of the waveguide. **c** A graphene *p-n* junction position as a function of gate voltage applied to one side of a waveguide. **d** Electric field of a *p-n* junction induced in graphene.

established methodology^{29,30} (see also Supplementary Note 2). A change in the gating voltage causes a lateral displacement of the *p-n* junction location within the graphene sheet (Fig. 1c). Moving the *p-n* junction, where the photoelectric signal is generated, across the gap between the gating electrodes allows one to accurately map the light field distribution across the gap. Note that the described field mapping approach, contrary to scanning near-field microscopy¹⁵, does not involve any moving parts and is thereby amenable to a very precise control of the scanning coordinate. The lateral size of *p-n* junction can be estimated from the built-in electric field distribution (Fig. 1d) and, for the 30 nm-thin hafnia separator, is ~ 20 nm, which is close to the previously reported values^{29,30}. It is worth mentioning that the calculated width of the *p-n* junction (Supplementary Note 2) changes around 40% for different gating voltages applied. However, the width was reasonably constant (~ 20 nm) in the region of the fast changes of the studied waveguide mode. In addition, Supplementary Note 2 calculates the “photo-active” width of the *p-n* junction in which electric fields are large enough to separate electron–hole pairs produced by light and which defines the spatial resolution of the technique. The calculated “photo-active” width (and hence the resolution of our technique) was below 20 nm for all gating voltages applied. Finally, we extracted the experimental spatial resolution of our technique from the measured data as described in Supplementary Note 6. This spatial resolution of light field mapping was also around 20 nm. This resolution can be easily improved by decreasing the thickness of a dielectric separator or lowering the temperature (see Supplementary Note 2) or using advanced gating electrode geometries.

Nanoscale light field imaging in plasmonic slot waveguides. For the experimental demonstration of our imaging approach, we have conducted the nanoscale electric field mapping of the gap surface plasmon (GSP) mode supported by a plasmonic slot waveguide. The plasmonic slot waveguide configuration, apart from allowing to squeeze the mode field down to nm-sized lateral dimensions³¹, has the advantage of fully exploiting the available dielectric space and thus making the best out of the confinement-loss trade-off¹⁰. It has been widely used in plasmon-empowered nanophotonics for demonstrating diverse ultra-compact components, ranging from branched and cross-shaped resonators³¹ to high-speed fibre-coupled electro-optical³² and ultrafast energy-efficient all-optical³³ modulators. The plasmonic slot waveguide configuration used for the demonstration of light field imaging with graphene (Fig. 2a) was designed to operate at telecom wavelengths³⁴. To fabricate the device, two pieces of graphene flakes were wet transferred on the silicon substrate that has a 1500 nm oxide layer on the top. Note that the dielectric silica layer should be sufficiently thick to minimize leakage of the GSP mode into the high refractive index silicon substrate. Graphene flakes were etched into two 4 μm -wide strips to serve as two detectors or as a modulator and a detector (see “Methods”). Then, a 30 nm-thick high refractive index dielectric (hafnium oxide) layer was deposited via electron beam evaporation above graphene strips to electrically isolate the graphene strips from the plasmonic waveguide structure used also for graphene gating. Hafnia was previously demonstrated to be a reliable dielectric layer for graphene gating with low voltages due to supercapacitance effect^{35,36}. Next, a 100 nm-thick silver waveguide structure with a 300 nm slot between the two strips was fabricated

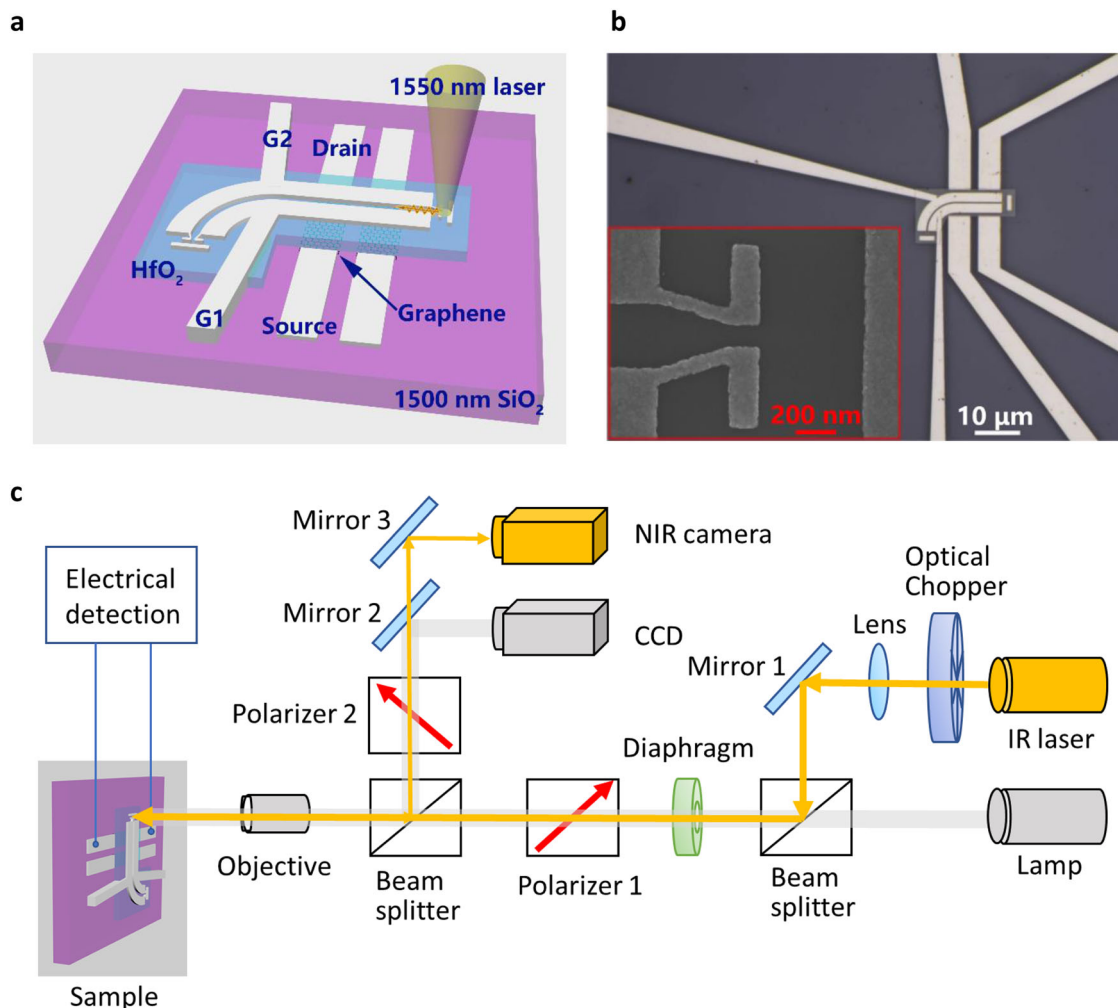


Fig. 2 Experimental setup. **a** Schematics of the antenna-coupled plasmonic waveguide device. Two pieces of graphene work separately for the optical modulation and electrical detection of the waveguide mode. **b** A microscope image of one device. Inset shows an enlarged picture of the nano-antenna and the reflector taken by scanning electron microscope. **c** An experimental setup. A lamp and CCD camera were used to locate the sample. A NIR camera was used to detect input and output signals and to measure the light modulation under gating. An optical chopper and lock-in was used to achieve electrical detection of light in the waveguide.

using electron beam lithography and lift-off process. During this procedure, 100 nm-thick silver contacts to the graphene flakes and the waveguide legs were also fabricated (Fig. 2b). The slot waveguide incorporates a 90° bend to enhance the visibility of the out-coupled (relatively weak) radiation as compared to that specular-reflected at the input coupler by using crossed polarizers (Supplementary Note 3). To efficiently interface free-space propagating (normal to the surface) radiation with the GSP mode supported by the slot plasmonic waveguide, two dipole nano-antennas with back reflectors³⁴ were fabricated near the waveguide terminations (inset in Fig. 2b). Finally, a 1.5 μm-thick layer of polymethyl methacrylate (PMMA) was used to cover the whole configuration in order to encapsulate the device and avoid oxidation.

The optical excitation of the resulting waveguide configuration involved a focused (40× objective with NA = 0.65) incident 1550-nm laser beam polarized parallel to the in-coupling antenna. The detection of the out-coupled radiation was performed in the cross-polarized configuration (Fig. 2c). Using InGaAs short-wave infrared (SWIR) camera, we controlled the excitation of the waveguide mode by monitoring the input and output light intensities (Supplementary Fig. 6b). At the same time, we were

able to measure a photo-current induced in graphene (between the source and drain contacts) as a function of the gate voltage in the presence/absence of light. This was performed using either light modulation with an optical chopper and lock-in detection, which provided the photocurrent response due to the GSP mode absorption by graphene, or direct measurements of the photocurrent with a source metre, which gave the dark and light responses.

The gating characteristics of graphene were determined by applying the same gate voltage to both waveguide sides G1 and G2 with a graphene strip being grounded (Fig. 3a). The range of applied gate voltages was determined by supercapacitor gating property of e-beam evaporated HfO₂^{35,36}. The ratio of the maximum and minimum values of the graphene sheet resistance was above 4 which suggests good quality of the graphene used. It is worth noting that the graphene was initially *p*-doped as the Dirac peak is shifted to the positive voltage (Fig. 3a). We also verified that the graphene strips interact with the GSP waveguide mode by realizing the modulation of output light intensity with graphene being gated to achieve the Pauli blocking effect³⁷. By applying a 1 Hz square-wave gate signal with 6 V amplitude and 1 V offset to both sides of the

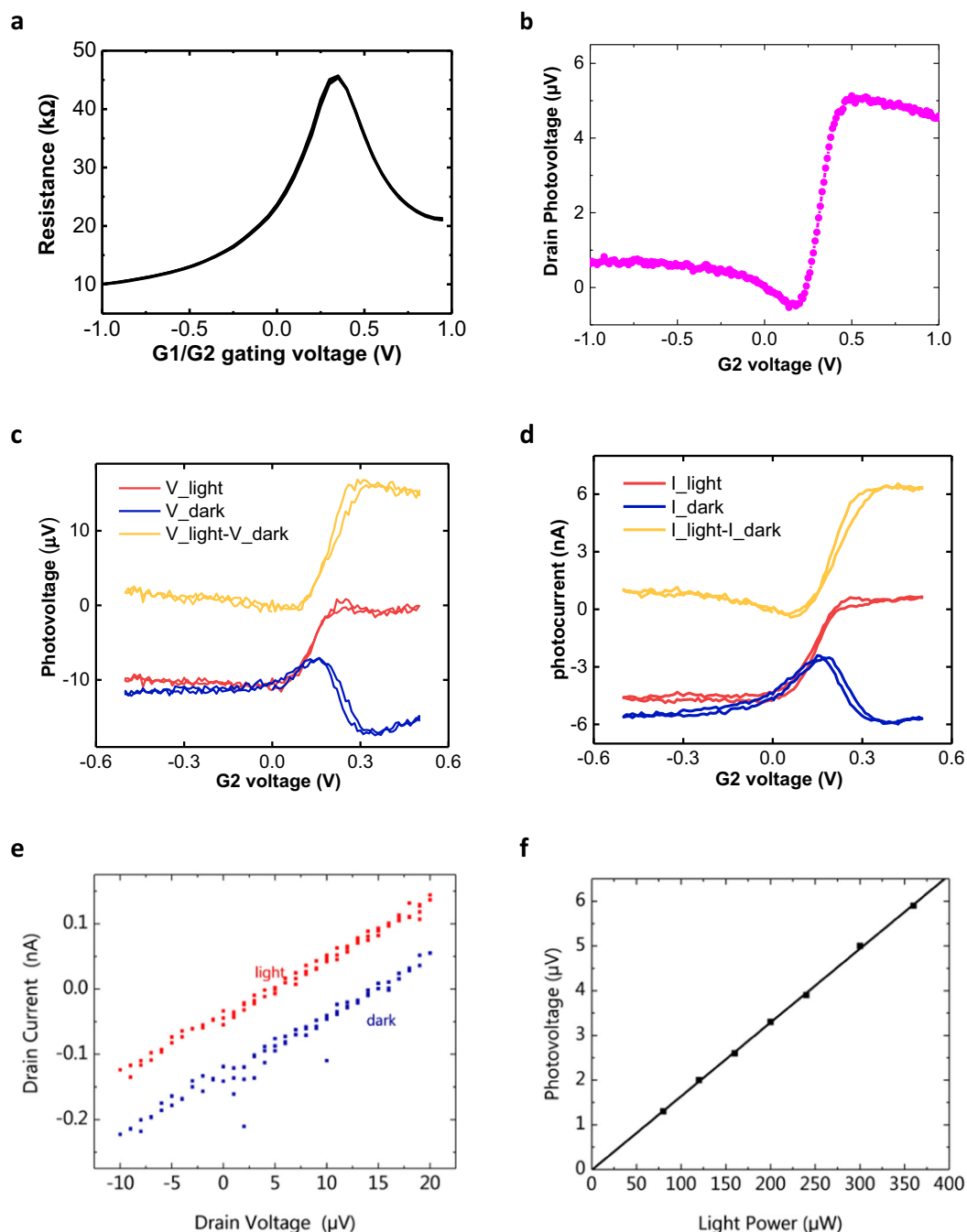


Fig. 3 Electrical mapping of light field in a plasmonic slot waveguide. **a** The resistance of graphene as a function of the gate voltage applied to both G1 and G2 contacts for a sample with a 30 nm HfO₂ dielectric layer. **b** A photovoltage measured between the source and drain of graphene as a function of the gate voltage G2 when the contact G1 is grounded. The photovoltage was measured with an optical chopper and lock-in amplifier. **c** A photovoltage (drain voltage in open circuit) and **d** a photocurrent (drain current in a short circuit) as a function of the gate voltage G2 with and without light input through the waveguide, measured directly with a source metre. Both the source and the G1 contact were connected to the ground. **e** Dependence of the photocurrent on the drain bias voltage of graphene with and without illumination. Both source and G1 are connected to ground, and 0.4 V gate voltage is applied to G2. **f** Linear dependence of the photovoltage on the incident light power with a fixed gate voltage of 0.4 V applied to G2 and G1 contact being grounded. The data for **a**, **b** and **c-f** were measured on two different samples with the same geometry.

waveguide, we observed a 12% modulation of the transmitted output light (Supplementary Fig. 6e). This modulation level corresponds to the modulation depth of 0.12 dB- μm^{-1} , which is significantly larger than those obtained previously with hybrid graphene plasmonic waveguide modulators^{23,35}, and assigned to strong change in graphene absorption due to Pauli blocking. It is worth noting that these measurements allowed us to establish

that Fermi level in graphene reaches half of the excitation energy (conditions for the Pauli blocking) at the applied gate voltage of 5.5 V.

The main result of our work, electrical mapping of light intensity with the help of graphene, was obtained with the gate voltage being applied to the contact G2 (while the contact G1 was grounded) to form a *p-n* junction in graphene underneath,

which could then be moved by adjusting the gate voltage (see Fig. 1c). Using the input laser light at the wavelength of 1550 nm and power of 0.5 mW, the corresponding photovoltage was measured (at zero applied bias between the source and drain contacts) with lock-in detection (chopping at 800 Hz) as a function of the gate voltage applied to G2 (Fig. 3b). The photovoltage being near zero for the gate voltages below 0.2 V (not large enough to induce *p-n* junction in graphene at the places with light fields) is seen to increase sharply for larger gate voltages, reaching the maximum value of $\sim 5 \mu\text{V}$ at 0.4 V gate voltage. The drain photovoltage measured as a function of the gate voltage (Fig. 3b) allowed us to restore the electromagnetic field profile of the GSP mode excited in the plasmonic slot waveguide as described in “Discussion”. Note that the maximum gate voltage applied and thereby maximum of the *p-n* junction displacement was restricted by the electric breakdown of the dielectric.

We have also measured both the photovoltage and photocurrent dependencies on the gate voltage directly with a source metre (i.e., without using the lock-in detection) under the light and dark conditions (i.e., with and without the incident light). Two representative runs (demonstrating the repeatability of measurements) are displayed for the light and dark photovoltages (Fig. 3c) and photocurrents (Fig. 3d) signals. Both light and dark photovoltages show a non-zero limit at negative voltages which is associated with the contact voltages. At the same time, the difference between the dark and light photovoltages (the yellow curve in Fig. 3c) follows the same behaviour as that observed with the lock-in measurements (Fig. 3b). The light and dark photocurrents measured at the conditions of zero applied bias voltage (Fig. 3d) behave similarly to the corresponding photovoltages (Fig. 3c). The dark current and voltage dependencies connected by the Ohm’s law reflect the gating characteristics of graphene strips (Supplementary Note 4 and Supplementary Fig. 7). Besides, both light and dark photocurrents show a linear dependence on the bias voltage between the source and the drain (from -10 to $20 \mu\text{V}$) provided the gate voltage applied to the contact G2 is constant (Fig. 3e). Finally, the photovoltage was measured to depend linearly on the incident light power (Fig. 3f) as one would expect for the photo-response governed by the photoelectric effect. It is worth mentioning that linear photo-response could also be observed for thermoelectric effect at some conditions^{25,38}. Calculations of the thermoelectric contribution in the linear approximation for our structures are provided in Supplementary Note 7.

Discussion

Light propagation and field distribution in our device were modelled with finite difference time domain (FDTD) simulations (Lumerical) for the experimental geometry and conditions (Supplementary Note 5), revealing details of the GSP mode propagation and attenuation in the waveguide (Fig. 4a). The simulated power transmission ratio $P_{\text{out}}/P_{\text{in}}$ was 0.12%, which is close to the experimentally measured ratio of 0.1%. To get more accurate values of electric field distribution of the studied GSP mode, we employed the two-dimensional (2D) mode analysis using the finite-element method (FEM) implemented in COMSOL software (“Methods”). The 2D distribution of electric field magnitude in the waveguide cross-section (Fig. 4b) represents a typical GSP mode field profile in a slot waveguide, with the electric field component E_x (across the slot and in the graphene plane) being strong and weakly varying (Fig. 4c) resembling the electrostatic field distribution in a capacitor.

The main contribution to the photo-response in our geometry comes from photoelectric effect in the *p-n* junction induced in

graphene by the gating voltage as discussed above. In order to recover the mode profile along the graphene from the photovoltage dependence on the gate voltage (Fig. 3b), one should verify linearity of the photo-response with respect to the mode power (Fig. 3f) and correlate the position of the graphene *p-n* junction and the gating voltage applied to contact G2 (Fig. 1c). With this information at hand, we were able to plot the intensity of the (GSP mode) electric field component in graphene plane as a function of the *p-n* junction position, obtaining thereby the GSP mode field profile in the plasmonic slot waveguide. Excellent agreement between the calculated and reconstructed plasmonic mode intensity profiles (Fig. 4d) demonstrates the success of electrical mapping of optical field intensity using graphene. The possible reason for a disagreement of profiles at large gating voltages (that were needed to move the *p-n* junction in graphene to the middle of the waveguide) is connected to larger leakage currents inside the dielectric which break simple capacitance relation between the applied voltage and the induced charges in the graphene sheet. It is worth adding that the thermoelectric effect was often claimed to be the main contributor to the generated by light signals in hybrid graphene/plasmonic systems^{25,38}. However, the calculations of the thermoelectric contribution in the linear approximation for our structures (provided in Supplementary Note 7) were not able to describe the measured data.

The spatial resolution of this mapping depends on the properties of the *p-n* junction induced in graphene. The spatial resolution of our measurements was extracted from comparison of the measured field profile with the calculated field distribution in Supplementary Note 6. This comparison yielded the Gaussian apparatus function with width of 9.5 nm and the resolution at the full width at half maximum of the response function of 22 nm. Since we applied the gating voltages of ~ 1 V, which is much smaller than 5.5 V necessary to achieve Pauli blocking in our devices, this implies that Pauli blocking did not affect the light absorption in the induced graphene *p-n* junction. Using the FDTD modelling we estimated the maximal photocurrent produced in the graphene *p-n* junction under our experimental conditions as ~ 3 nA, which is close to the observed photocurrents (Supplementary Note 5). Finally, it is worth stressing again that graphene does not significantly perturb electromagnetic field distributions due to small light absorption. Our light-field imaging method is especially useful for characterization of strongly confined optical modes supported by planar nanophotonic circuitry, since it allows natural integration of intermediate graphene monolayers and gate electrodes (which, potentially, can also be made from graphene, thus, making the whole system even less invasive). An addition of a graphene layer to a nanostructure is not a difficult process: it requires several additional steps in the fabrication procedure or one transfer step if we apply graphene to a ready-made structure. The measurement procedure then requires only simple optics and a source metre and, hence, is open to many researchers. In our work, we have demonstrated only one-dimensional (1D) imaging of plasmonic light fields. We note that electric gates, necessary for implementation of our method, could have other symmetry, e.g., we can use circular nanoparticles and circular gates, *x-y* gates, or we can place studied nanoparticles (even made of dielectric) inside the plasmonic slot waveguide and compare the field profiles with and without nanoparticles. We can also envisage a creation of complex moving *p-n* junction by a proper electron illumination. Even at the simplest 1D realization described in our work, our technique is already capable of achieving what none of existing microscopy technique can achieve and we have no doubts that it can be developed further.

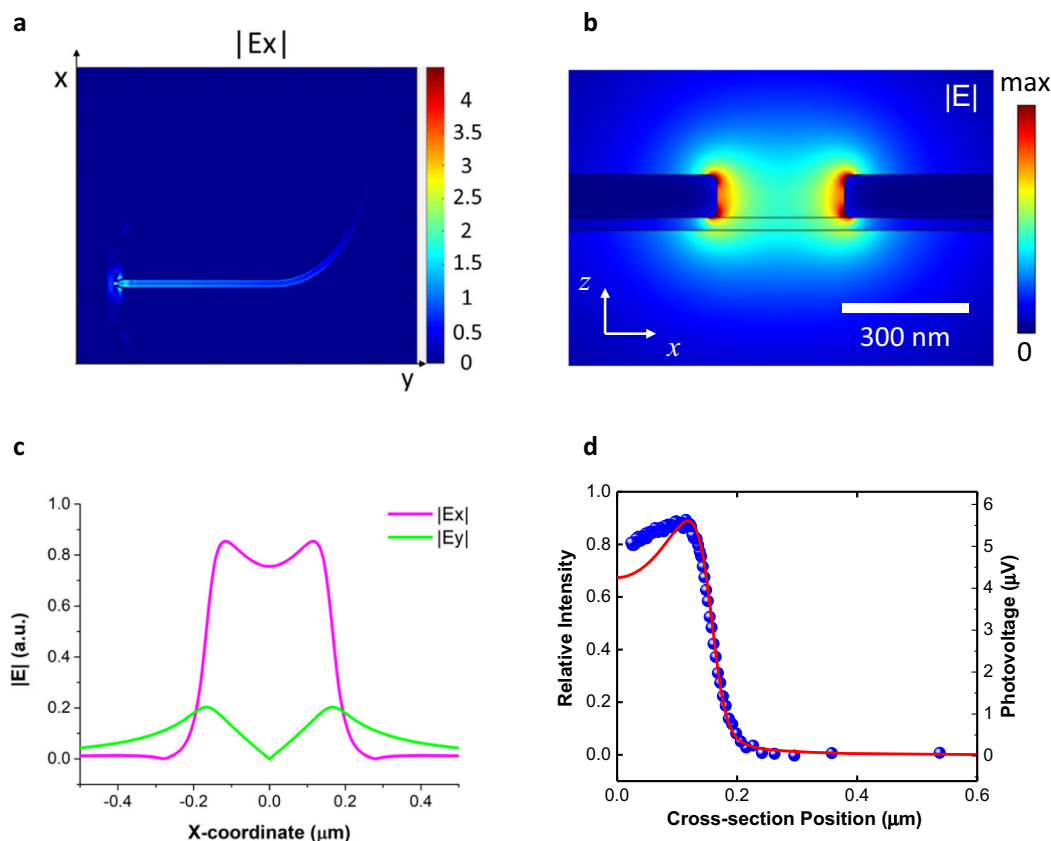


Fig. 4 Comparison of light field profiles with theory. **a** Simulated electric field distribution excited by a laser beam (wavelength of 1550 nm) that falls onto the input antenna (taken in the plane of the waveguide at the half-height of the waveguide and calculated with the help of Lumerical FDTD solutions). **b** Simulated electric field distribution in the cross-section of the plasmonic slot waveguide calculated with the help of Comsol software. **c** The line-scan of the norm of electric field calculated at the graphene position. **d** Comparison of the simulated field profile in the plasmonic slot waveguide (the red solid line) with the reconstructed profile obtained with a p - n junction moved in graphene by gating (the blue circles).

Conclusion

We have suggested and experimentally realized the electromagnetic field mapping based on the photo-detection with a p - n junction induced and moved inside graphene by an external gate voltage. The spatial resolution of this electrical, rather than mechanical, scanning technique is determined by the p - n junction width of ~ 20 nm which can further be improved by decreasing the thickness of the gating dielectric. The developed approach is demonstrated with mapping the electric field distribution of a strongly confined plasmonic slot-waveguide mode at telecom wavelengths, resulting in the mode profile found in excellent agreement with numerical simulations. Importantly, the developed configuration exhibited also good electro-optical modulation characteristics, featuring the modulation depth of $0.12 \text{ dB}\cdot\mu\text{m}^{-1}$ at the gate voltage amplitude of 6 V. Our method of non-invasive light mapping provides a fresh paradigm in nanoscale optical characterization that ensures extremely high spatial resolution and precision, offering at the same time promising opportunities for nanoscale plasmonic on-chip devices.

Methods

Fabrication. To fabricate the devices, a piece of graphene grown on copper by a chemical vapour deposition process was transferred on a Si substrate with top $1.5 \mu\text{m}$ thick SiO_2 layer using a standard wet-transfer method: a layer of PMMA was firstly spin-coated on the graphene, and then the copper underneath was etched in an ammonium persulfate solution. The floating membrane was then moved to deionized water with the help of a clean Si chip to remove the ammonium persulfate residue. Finally, the PMMA/graphene membrane was fished with the substrate. After that, it was left to dry for 24 h, and after drying, it was baked in

a hot plate at 170°C (improving adhesion between graphene and substrate) for 15 min and then bathed in acetone for 10 min to remove the PMMA. The sample was then put in isopropanol solvent for 10 min to clean residual acetone and dried with a nitrogen gun. The area with good graphene quality was located by optical microscopy. Electron beam lithography and O_2 :Ar plasma etch were used to define two graphene stripes on the substrate. The dielectric layer pattern was defined by electron beam lithography. Then, 30 nm hafnium oxide was deposited on the substrate above two graphene stripes with the help of electron beam evaporation, which was performed by Moorfield deposition system at a speed of 0.6 \AA/s . After the lift-off procedure, the sample was cleaned with isopropanol alcohol (IPA) and deionized water. The waveguide structure and contacts pattern were again defined by a third electron beam lithography, using a 210 nm thick layer of PMMA and a high-resolution 100 kV beam. The exposed areas were developed at 5°C in methyl isobutyl ketone:IPA mixture with ratio 1:3 for 40 s and then IPA for 20 s. 1 nm Cr as adhesion layer and 100 nm Ag were evaporated with Moorfield electron beam deposition system, with a high deposition rate of $0.9 \text{ nm}\cdot\text{s}^{-1}$ for the silver deposition. After the final lift-off, the waveguide structures were imaged with a scanning electron microscope (SEM). Then, the whole device was spin-coated by a $1.5 \mu\text{m}$ thick PMMA layer to protect silver from oxidation. More details on sample fabrications, measurement procedures, and results can be found in ref. ³⁹.

COMSOL simulations. Mode analysis was performed using FEM implemented in RF module of COMSOL software (version 5.3). As can be seen in Fig. 4b, edges of silver electrodes were rounded with a 20 nm radius of curvature to avoid artificial singularities and influence of mesh discretization, which should better represent the fabricated geometry. All material properties were the same as in 3D FDTD simulations, and graphene layer was assumed to have no influence on the mode profile and, thus, not included into simulations. A standard triangular mesh was applied, with a maximum mesh element size of 10 nm inside silver and $(190 \text{ nm})/n$ everywhere else, where n stands for the refractive index of correspondent material. The mesh of the line, corresponding for the position of graphene, was refined to decrease the mesh size down to ~ 1 nm. The whole simulation domain size was $14 \times 14 \mu\text{m}^2$, with perfect electric conductor boundary conditions. The convergence of simulations was verified by

varying the meshing and domain size. We also verified the waveguide light profile with the help of an alternative FDTD software³⁹.

Data availability

The data that support the findings of this study are available from the corresponding author ANG upon reasonable request.

Received: 5 February 2022; Accepted: 15 June 2022;

Published online: 29 June 2022

References

- Novotny, L. & Hecht, B. *Principles of Nano-Optics* (Cambridge University Press, 2019).
- Zayats, A. V., Smolyaninov, I. I. & Maradudin, A. A. Nano-optics of surface plasmon polaritons. *Phys. Rep.* **408**, 131–314 (2005).
- Lal, S., Link, S. & Halas, N. J. Nano-optics from sensing to waveguiding. *Nat. Photonics* **1**, 641–648 (2007).
- Maier S. A. *Plasmonics: Fundamentals and Applications* (Springer, 2007).
- Prodan, E., Radloff, C., Halas, N. J. & Nordlander, P. A hybridization model for the plasmon response of complex nanostructures. *Science* **302**, 419 (2003).
- Halas, N. J., Lal, S., Chang, W.-S., Link, S. & Nordlander, P. Plasmons in strongly coupled metallic nanostructures. *Chem. Rev.* **111**, 3913–3961 (2011).
- Kravets, V. G., Kabashin, A. V., Barnes, W. L. & Grigorenko, A. N. Plasmonic surface lattice resonances: A review of properties and applications. *Chem. Rev.* **118**, 5912–5951 (2018).
- Fang, N., Lee, H., Sun, C. & Zhang, X. Sub-diffraction-limited optical imaging with a silver superlens. *Science* **308**, 534 (2005).
- Zhang, X. & Liu, Z. Superlenses to overcome the diffraction limit. *Nat. Mater.* **7**, 435–441 (2008).
- Gramotnev, D. K. & Bozhevolnyi, S. I. Plasmonics beyond the diffraction limit. *Nat. Photonics* **4**, 83–91 (2010).
- Koppens, F. H. L., Chang, D. E. & Javier Garcia de Abajo, F. Graphene plasmonics: A platform for strong light–matter interactions. *Nano Lett.* **11**, 3370–3377 (2011).
- Grigorenko, A., Polini, M. & Novoselov, K. Graphene plasmonics. *Nat. Photonics* **6**, 749–758 (2012).
- Low, T. et al. Polaritons in layered two-dimensional materials. *Nat. Materials* **16**, 182–194 (2017).
- Born, M. & Wolf, E. *Principles of Optics* (Cambridge University Press, 1980).
- Rotenberg, N. & Kuipers, L. Mapping nanoscale light fields. *Nat. Photonics* **8**, 919–926 (2014).
- Hulst, H. C. & van de Hulst, H. C. *Light Scattering by Small Particles* (Dover Publications, 1981).
- Taboada-Gutiérrez, J. et al. Broad spectral tuning of ultra-low-loss polaritons in a van der Waals crystal by intercalation. *Nat. Materials* **19**, 964–968 (2020).
- García de Abajo, F. J. Optical excitations in electron microscopy. *Rev. Mod. Phys.* **82**, 209–275 (2010).
- Cang, H. et al. Probing the electromagnetic field of a 15-nanometre hotspot by single molecule imaging. *Nature* **469**, 385–388 (2011).
- Willems, K. A. Super-resolution imaging of SERS hot spots. *Chem. Soc. Rev.* **43**, 3854–3864 (2014).
- Hillenbrand, R. & Keilmann, F. Optical oscillation modes of plasmon particles observed in direct space by phase-contrast near-field microscopy. *Appl. Phys. B* **73**, 239–243 (2001).
- Nair, R. R. et al. Fine structure constant defines visual transparency of graphene. *Science* **320**, 1308–1308 (2008).
- Ansell, D. et al. Hybrid graphene plasmonic waveguide modulators. *Nat. Commun.* **6**, 8846 (2015).
- Echtermeyer, T. J. et al. Strong plasmonic enhancement of photovoltage in graphene. *Nat. Commun.* **2**, 458 (2011).
- Gabor, N. M. et al. Hot carrier–assisted intrinsic photoresponse in graphene. *Science* **334**, 648–652 (2011).
- Freitag, M., Low, T., Xia, F. & Avouris, P. Photoconductivity of biased graphene. *Nat. Photonics* **7**, 53–59 (2013).
- Mahan, G. D. The Benedicks effect: Nonlocal electron transport in metals. *Phys. Rev. B* **43**, 3945–3951 (1991).
- Grigorenko, A. N., Nikitin, P. I., Jelski, D. A. & George, T. F. Thermoelectric phenomena in metals under large temperature gradients. *J. Appl. Phys.* **69**, 3375–3377 (1991).
- Chaves, F. A., Jiménez, D., Santos, J. E., Bøggild, P. & Caridad, J. M. Electrostatics of metal–graphene interfaces: Sharp p–n junctions for electron-optical applications. *Nanoscale* **11**, 10273–10281 (2019).
- Lee, G.-H., Park, G.-H. & Lee, H.-J. Observation of negative refraction of Dirac fermions in graphene. *Nat. Phys.* **11**, 925–929 (2015).
- Raza, S. et al. Electron energy-loss spectroscopy of branched gap plasmon resonators. *Nat. Commun.* **7**, 13790 (2016).
- Ayata, M. et al. High-speed plasmonic modulator in a single metal layer. *Science* **358**, 630 (2017).
- Ono, M. et al. Ultrafast and energy-efficient all-optical switching with graphene-loaded deep-subwavelength plasmonic waveguides. *Nat. Photonics* **14**, 37–43 (2020).
- Thomaschewski, M., Yang, Y. & Bozhevolnyi, S. I. Ultra-compact branchless plasmonic interferometers. *Nanoscale* **10**, 16178–16183 (2018).
- Rodriguez, F. J., Aznakayeva, D. E., Marshall, O. P., Kravets, V. G., Grigorenko, A. N. Solid-state electrolyte-gated graphene in optical modulators. *Adv. Mater.* **29**, 1606372 (2017).
- Aznakayeva, D. E., Rodriguez, F. J., Marshall, O. P. & Grigorenko, A. N. Graphene light modulators working at near-infrared wavelengths. *Opt Express* **25**, 10255–10260 (2017).
- Wang, F. et al. Gate-variable optical transitions in graphene. *Science* **320**, 206 (2008).
- Cai, X. et al. Sensitive room-temperature terahertz detection via the photothermoelectric effect in graphene. *Nat. Nanotechnol.* **9**, 814–819 (2014).
- Yu, T. *Materials and Nanostructures for Light-Matter Interactions in 2D*. PhD Thesis, University of Manchester (2021).

Acknowledgements

We acknowledge the support from the EU Graphene Flagship grant Core 3 (881603) and Graphene NOWNANO CDT programme funded by EPSRC grant EP/L01548X/1. F.S. was funded by European Graphene Flagship Project ERC Synergy grant Hetero2D. S.I.B. acknowledges the support from the Villum Kann Rasmussen Foundation. V.A.Z. acknowledges the financial support from Villum Fonden (Grant No. 16498).

Author contributions

A.N.G. conceived the project. A.N.G., S.I.B., and K.S.N. guided the project. T.Y., F.R., F.S., and V.G.K. made the samples and characterized them. T.Y. and F.R. performed optical measurements. S.I.B., V.A.Z., and T.Y. performed the modelling of waveguide modes. A.N.G. and K.S.N. contributed to the theory of *p-n* junctions. All authors contributed to discussions and manuscript preparation.

Competing interests

The authors declare no competing interests.

Additional information

Supplementary information The online version contains supplementary material available at <https://doi.org/10.1038/s43246-022-00264-0>.

Correspondence and requests for materials should be addressed to Alexander N. Grigorenko.

Peer review information *Communications Materials* thanks the anonymous reviewers for their contribution to the peer review of this work. Primary Handling Editor: Aldo Isidori.

Reprints and permission information is available at <http://www.nature.com/reprints>

Publisher's note Springer Nature remains neutral with regard to jurisdictional claims in published maps and institutional affiliations.



Open Access This article is licensed under a Creative Commons Attribution 4.0 International License, which permits use, sharing, adaptation, distribution and reproduction in any medium or format, as long as you give appropriate credit to the original author(s) and the source, provide a link to the Creative Commons license, and indicate if changes were made. The images or other third party material in this article are included in the article's Creative Commons license, unless indicated otherwise in a credit line to the material. If material is not included in the article's Creative Commons license and your intended use is not permitted by statutory regulation or exceeds the permitted use, you will need to obtain permission directly from the copyright holder. To view a copy of this license, visit <http://creativecommons.org/licenses/by/4.0/>.

© The Author(s) 2022